

# Pulsar twinkling and relativity

Isabelle A. Grenier\* and Alice K. Harding†

\*AIM, Service d'Astrophysique, CEA Saclay, 91191 Gif/Yvette, France

†NASA Goddard Space Flight Center, Greenbelt, MD 20771, USA

**Abstract.** The number of pulsars with detected emission at X-ray and  $\gamma$ -ray energies has been steadily growing, showing that beams of high-energy particles are commonly accelerated in pulsar magnetospheres, even though the location and number of acceleration sites remain unsettled. Acceleration near the magnetic poles, close to the polar cap surface or to higher altitudes in the slot gap along the last open field lines, involves an electric field component due to inertial-frame dragging. Acceleration can also take place in the outer magnetosphere where charge depletion due to global currents causes a large electric field along the magnetic field lines. All models require a detailed knowledge of the open magnetosphere geometry and its relativistic distortions. Observational trends with age, spin-down power and magnetic field as well as population synthesis studies in the Galactic disc and the nearby Gould Belt provide useful, however not yet conclusive, constraints on the competing models.

## INTRODUCTION

Pulsar twinkling is all relative. It depends on the shape of the pulsar magnetic field and the observer's point of view, on the metric near the neutron star and on retarded potentials and aberration of light in the outer magnetosphere. General and special relativity are involved at three stages: (1) for the unipolar inductor to extract charges and draw currents above the polar caps in dragged inertial frames; (2) to distort the magnetic field, thus affecting the pair cascading efficiency and the high-energy curvature radiation spawned by the primary charges; (3) to control the location and extent of the accelerating sites (gaps), thus lightcurve morphologies and polarization patterns. The overall flux and spectral distributions predicted as input to population synthesis studies are therefore quite sensitive to these effects.

Over 1560 radio pulsars have been discovered with periods ranging from milliseconds to seconds according to their history, and with spin-down powers spanning 10 orders of magnitude, from  $10^{21}$  to  $10^{31}$  W. The bulk of the population is middle-aged, around  $10^{6-7}$  years, with canonical fields near  $10^8$  T. Billion-year old millisecond pulsars have weak  $10^{4-5}$  T fields. The slow  $10^{4-6}$  year-old magnetars have supercritical fields of  $10^{10-11}$  T. Pulsars seen at high energy often have large fields in their outer magnetosphere, either because of their intense stellar field, as in anomalous X-ray pulsars, or because of the compactness of their magnetosphere, as in ms pulsars, or their youth for  $\gamma$ -ray pulsars. The latter are ostensibly younger than several  $10^5$  years because of the limited sensitivity of the current  $\gamma$ -ray telescopes. Despite the large size of the radio sample, little is known about the coherent process responsible for the radio pulses which consist of a core component near the polar cap and a hollow cone component which probably takes place at several tens of stellar radii above the polar cap ( $r_{\text{radio}}/R \sim 40 v_{\text{GHz}}^{-0.26} P^{0.3}$  at frequency  $\nu_{\text{GHz}}$  in GHz, for a neutron star radius  $R$  and period  $P$  in seconds [27]). More straightforward, incoherent processes, like curvature and synchrotron radiation and Compton scattering, give rise to the optical, X-ray and gamma-ray pulses.

The observed pulsed emission depends on a small set of parameters: the pulsar angular velocity  $\Omega$ , its spin-down power  $\dot{E}_{\text{psr}} = I\Omega\dot{\Omega}$  for a moment of inertia  $I$ , its characteristic age  $\tau = \Omega/(2\dot{\Omega})$ ; the inclination angle  $\alpha$  of its magnetic field to the rotation axis and the observer's viewing angle  $\zeta$  to the same axis; the radius of the light cylinder  $R_{\text{LC}} = c/\Omega$  where the corotation velocity reaches the speed of light; the intensity of the surface magnetic field  $B_p$  at the pole; the polar cap half angle  $\sin \theta_{\text{PC}} = (R\Omega/c)^{1/2}$ . The Deutsch vacuum solution[6] for the field is often adopted. The near-dipole geometry has been recently confirmed by [28].

## ELECTRODYNAMICS AND ACCELERATION

Rotating, magnetized neutron stars are natural unipolar inductors, generating huge electric fields in vacuum ( $\vec{E} = -(\vec{\Omega} \wedge \vec{r}) \wedge \vec{B}$ ) and building a large surface charge. However, Goldreich & Julian [12] noted that the electric field component parallel to the magnetic field,  $E_{\parallel}$ , at the stellar surface can pull charges out of the star against gravity to build a force-free density in the magnetosphere. Wherever the charge can reach the Goldreich-Julian (GJ) charge density,  $\rho_{GJ} \simeq -2\epsilon_0 \vec{\Omega} \cdot \vec{B}$ , it is able to short out  $E_{\parallel}$ , and both charges and dipole field will corotate with the star. Corotation must break down at large distances from the neutron star due to particle inertia. Global magnetospheric simulations [34, 37] have not yet been able to show whether and how a pulsar magnetosphere reaches the nearly force-free (ideal MHD) state envisioned by Goldreich & Julian, in particular how the large amount of charges are supplied to meet the force free conditions. Clearly, particle acceleration requires at least some local departure from force-free conditions. So, a real pulsar magnetosphere must exist somewhere between the idealized vacuum and force-free states we have been able to study so far on a global scale. Pulsar particle acceleration has so far been studied on a local scale and two types of accelerator, polar cap and outer gap, have received the most attention.

### Polar cap and slot gap accelerators

In polar cap accelerators, voltage develops along open field lines near and above the polar cap surface. The two main subclasses are vacuum gap models [36], where charges are trapped in the neutron star surface layers by binding forces and a region of vacuum forms above the surface, and space-charge limited flow (SCLF) models [2], where charges are freely emitted from the surface layers and a voltage develops due to the small charge deficit between the real charge density  $\rho$  and  $\rho_{GJ}$  according to  $\vec{\nabla} \cdot \vec{E}_{\parallel} = (\rho - \rho_{GJ})/\epsilon_0$ . The two types of accelerators differ only by the surface boundary condition on the charge density, where  $\rho(R) = 0$  for the vacuum gap, and  $\rho(R) = \rho_{GJ}$  for SCLF accelerators. For vacuum gaps,  $E_{\parallel} = \Omega B_p R$  is the full vacuum value at the surface. For SCLF accelerators,  $E_{\parallel} = 0$  at the surface but it grows with increasing  $r$  because  $\rho$ , which must satisfy charge continuity along each field line, decreases as  $r^{-3}$  while  $\rho_{GJ}$  decreases more slowly. The form of  $E_{\parallel}$  in SCLF accelerators is thus sensitive to the detailed distribution of the charge density, which depends both on the open field line geometry as well as the compactness of the neutron star. At altitudes  $\{z \ll \theta_{PC}, z \gg \theta_{PC}\}$ , with  $z \equiv (r/R - 1)$  being the height above the surface,

$$E_{\parallel} \simeq B_p \theta_{PC}^2 \left[ \left\{ z, \theta_{PC}^2 \left( \frac{r}{R} \right)^{-4} \right\} \kappa \cos \alpha + \left\{ z, \theta_{PC}^2 \left( \frac{r}{R} \right)^{-1/2} \right\} \frac{\theta_{PC}}{2} \sin \alpha \cos \varphi \right] \left[ 1 - \left( \frac{\theta}{\theta_{PC}} \right)^2 \right] \quad (1)$$

[33, 16], where  $\theta$  and  $\varphi$  are the magnetic polar and azimuth angles,  $\kappa = 2GI/(c^2 R^3)$  is the stellar compactness parameter, and  $I$  the neutron star moment of inertia. The first term in Eqn (1) is due to inertial frame dragging near the neutron star surface, and dominates for small  $r$  and low inclination, while the second term is due to the flaring of the field lines.

The potential drop available for particle acceleration is limited by the development of electron-positron pair cascades which screen the  $E_{\parallel}$ . In vacuum gap models, the pair cascade is initiated when the gap height becomes comparable to the photon mean free path for one-photon pair creation in the strong magnetic fields, and causes a sudden discharge of the vacuum. The potential drop in the gap thus oscillates between  $V_{vg} \sim \Omega B_p (R \theta_{PC})^2 / 2$  and 0. In SCLF models, the pair cascades do not cause a discharge, but develop only at the upper boundary of the accelerator, screening the  $E_{\parallel}$  in a relatively thin region above a pair formation front (PFF) by trapping a small fraction of positrons that accelerate downward. These accelerators can thus maintain a steady current of upwardly accelerating electrons, at  $j_{\parallel}^- \simeq c \rho_{GJ}$ , and a downward current of positrons, at  $j_{\parallel}^+ \ll c \rho_{GJ}$ , which heat the polar cap. The accelerator voltage is determined by the height of the PFF, which is again roughly comparable to the pair creation mean-free path.

The geometry of the polar cap accelerator is determined by  $E_{\parallel}$  and the physics of pair screening. Near the magnetic pole,  $E_{\parallel}$  is relatively strong and the PFF is very near the neutron star surface. But at the polar cap rim, which is assumed to be a perfectly conducting boundary,  $E_{\parallel}$  vanishes. Near this boundary, the electric field is decreasing and a larger distance is required for the electrons to accelerate to the Lorentz factor needed to radiate photons energetic enough to produce pairs. The PFF thus moves up and curves upward as the boundary is approached, forming a narrow slot gap near the last open field line [1]. Since  $E_{\parallel}$  is unscreened in the slot gap, particles continue to accelerate and radiate to high altitude along the last open field lines. High-energy radiation can therefore come from low-altitude ( $r < 2R$ ) pair

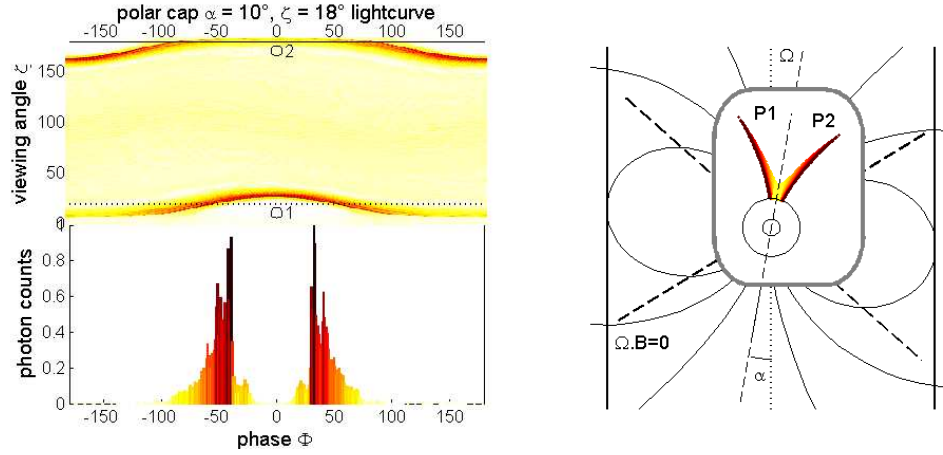


**FIGURE 1.** Phase plot, sample lightcurve, and a sketch of the accelerator location for the polar cap model, for a typical inclination angle  $\alpha = 10^\circ$ . The central zoom gives the gap extent relative to the star size. The shading in the lightcurve and gap sketch is the same. The phase plot illustrates the change in lightcurve as seen by different observers and the aperture of the pulsed beams.

cascades near the pole [7], higher-altitude ( $r < (3 - 4)R$ ) pair cascades on the inner edge of the slot gap [30], and high altitude ( $r \sim (0.1 - 0.8)R_{LC}$ ) radiation from primary particles in the extended slot gap [31].

## Outer gap accelerators

Outer gap accelerator models [4, 35] focus on regions in the outer magnetosphere that cannot fill with charge, since they lie along open field lines crossing the null surface,  $\vec{\Omega} \cdot \vec{B} = 0$ , where  $\rho_{GJ}$  reverses sign. Charges pulled from the polar cap cannot populate the region between the null surface and the light cylinder, and a vacuum gap forms. This assumes of course that the charges coming from the polar cap on these field lines do not undergo enough pair cascading to screen the outer gap. If outer gaps form, they can accelerate particles to high energy and the radiated  $\gamma$ -rays can produce pairs by interacting with thermal X-rays from the neutron star surface. The density of such X-ray photons is very small in the outer gaps, but is enough to initiate pair cascades since the newborn pairs accelerate in the gap, radiate, and produce more pairs. The gap size is limited by the pair cascades, which screen the gap electric field both along and across field lines, thus determining the emission geometry. Young pulsars, having hotter polar caps and higher vacuum electric fields, tend to have narrow gaps stretching from near the null surface to near the light cylinder [3] while the gaps of older pulsars, having lower electric fields, are much thicker and grow with age [42]. When the gap fills the whole outer magnetosphere (at  $\tau \gtrsim 10^7$  yr) it ceases to operate, so that not all radio pulsars can emit  $\gamma$  rays. Death lines in  $P$ - $\dot{P}$  space predict which pulsars can sustain outer gaps, depending on whether the X-ray photon field comes from cooling of the whole stellar surface or from polar caps heated by the energy deposited by the return flux of charges [43].

Recent outer gap models [40] solve Poisson's Equation in two dimensions (along and across the magnetic field). Such 2D models derive a somewhat different gap geometry than the classic one-dimensional models. Depending on the amount of current flow into the gap, of order 10-20 % of the GJ current, the gap can be long and narrow or wide and thick. Such current flow is required for the gap to produce a sufficient high-energy luminosity [25]. The 2D gaps can extend below the null charge surface and to a maximum height of about  $0.8R_{LC}$ , in contrast to the classic outer gaps that were assumed to extend from the null surface to  $R_{LC}$ .

## CASCADES AND RADIATION

The polar cap/slot gap and the outer gap models both use curvature radiation to produce the primary  $\gamma$  rays with energies around 50 GeV to initiate the cascades [24] [7], but they differ in the pair creation process: magnetic one-photon production in the intense field at low altitude, and two-photon creation in the outer regions. Due to screening of the  $E_{\parallel}$  by the pair cascades, the maximum Lorentz factor  $\gamma_{e,max}$  saturates at several  $10^7$  for both the polar cap and outer gap and is very insensitive to  $\Omega$  and  $\dot{\Omega}$ . The following stages of the photon- $e^{\pm}$  shower use the same radiation processes, namely synchrotron radiation which is more efficient in the inner regions, and inverse Compton scattering of the stellar thermal radiation.

Polar cap pair cascades are initiated by primary curvature radiation (CR), in the case of the young pulsars ( $\tau \lesssim 10^7$  yr), and by inverse-Compton scattering (ICS) of stellar thermal X-rays by primary electrons [38], for older pulsars that cannot produce pairs from CR because of the weaker  $E_{\parallel}$  and straighter field lines [17]. Secondary to primary number ratios from CR cascades reach  $10^3 - 10^4$  [7], but only  $1 - 100$  for ICS cascades [23]. Radio emission is predicted to cease when a pulsar can no longer even produce pairs from ICS [18]. The polar cap cascade spectra of young, high-field pulsars show super-exponential high-energy cutoffs at energies between 20 MeV and 20 GeV due to magnetic pair attenuation. The cutoff energy is also influenced by GR effects such as light bending and photon red-shifts [13]. The cutoff energy is expected to be lower on the leading edge of the pulse due to rotationally induced asymmetries in the pair absorption (larger angles between the photons and field lines on the leading side) [9]. The predicted spectra of millisecond pulsars with very low surface fields are not attenuated and may extend as high as 50 GeV [20].

Outer gap cascades are initiated by CR from primaries and can be as rich as the polar cap cascades. Flux and spectra are quite sensitive to attenuation by pair production and to the feedback between the heated polar caps and the cascade development [40]. A distinctive feature of the outer gap is the significant 0.1-10 TeV emission component due to Compton scattering of soft IR and X-rays by the gap accelerated particles. The outer gap and slot gap spectra show simple exponential cut-offs due to the radiation-reaction limit of the particle energy. The return particle current appearing near the edge of the open volume in global MHD simulations [37] could have some effect of the structure of both outer gaps and slot gaps.

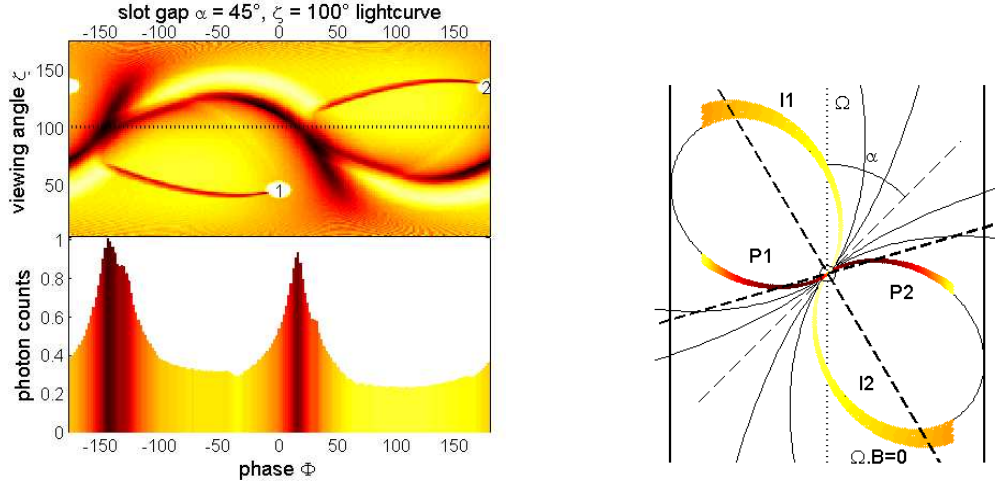


**FIGURE 2.** Same as Figure 1 for the slot gap model, for a typical inclination angle  $\alpha = 45^\circ$ .

## GEOMETRY AND PHASE

Assuming outward radiation tangent to the field lines, lightcurve morphologies depend on general relativity (field distortion and light bending near the star surface) and on special relativity (light aberration, time-of-flight delays and field retardation near the light cylinder). Aberration and time-of-flight produce phase shifts of comparable magnitudes  $\Delta\Phi \sim -r/R_{LC}$  in radiation emitted at different altitudes. On the leading side, these phase shifts add up to spread photons emitted at various altitudes over  $\Delta\Phi \sim 0.4$  in phase. On the trailing side, photons emitted later at higher

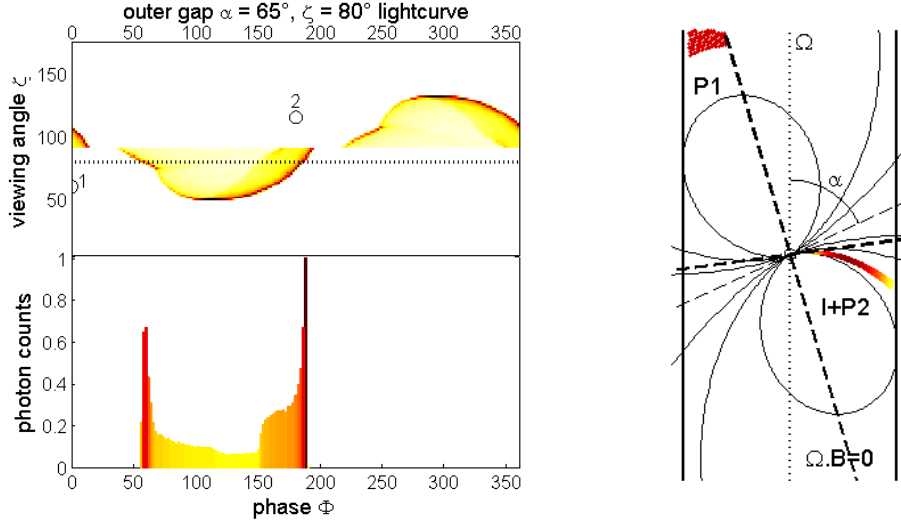


**FIGURE 3.** Same as Figure 1 for the outer gap model, for a typical inclination angle  $\alpha = 65^\circ$ . The outer gap lies along field lines with  $\theta = 0.85\theta_{PC}$  as in [5].

altitudes catch up with those emitted earlier at lower altitude. They arrive at an observer within a small phase range  $\Delta\Phi \sim 0.1$  and produce caustics in the phase plot and light curve [10, 5]. These effects dominate over the small degree of sweep-back of the retarded field lines near the light cylinder ( $\Delta\Phi \sim 1.2(r/R_{LC})^3 \sin^2\alpha$ ) [8]. The gravitational bending of light paths near the surface is small and compensated by the reduced size of the polar cap in a Schwarzschild metric ( $\theta_{PC}^R = \theta_{PC}(1 + 2GM/Rc^2)^{-1/2}$ ) [13]. The shape of the open volume depends on the pulsar obliquity and retarded field (the polar cap radius varies with azimuth around the pole), the pulsar age (the polar cap shrinks with age as  $\sin(\theta_{PC}) \propto \Omega^{1/2}$  and the light cylinder expands as  $R_{LC} \propto \Omega^{-1}$ ), and to a lesser degree, on the reduced polar cap in a curved space-time. Currents can easily further distort the weak magnetic field in the outer magnetosphere, but also near the star. The lines swell along the rotation axis under the drift ( $\vec{E} \wedge \vec{B}$ ) current and they curl more than the rotational sweep-back because of the returning polar current (if electrons are extracted) [32]. All these effects strongly affect the width and symmetry about the pole of the polar cap beam as well as the slot and outer gap lengths and their peak phases for radiation.

Figures 1 to 3 try to capture these effects. They show the dependence of photon intensity on phase for different observer viewing angles, for the three models with typical magnetic inclinations. The dipole sketches (simple, unretarded dipoles) qualitatively illustrate the gaps location and extent. The grey shading outlines the emerging photon phase in the lightcurves as well as across the gaps.

A single polar-cap beam can produce a variety of pulse profiles with any peak separation between 0 and  $180^\circ$  as long as  $\alpha \sim \zeta \leq 30^\circ$  (Fig. 1). Because  $E_{||}$  fades away near the perfectly conducting edge of the open volume, the gap is shorter near the pole ( $0.5R_*$ ) and extends to higher altitude near the rim. Cascade synchrotron emission is brighter along the more curved lines near the rim. Faint and soft "off-beam" curvature radiation from the primary particles above the gap can be seen outside the main beam, in particular at large viewing angles [19]. Off-beam emission is softer because it originates inside the open volume at large altitudes along field lines with larger curvature radii, and because the particles have lost much of their initial energy.

Slot gap emission fills the whole sky and all phases in a lightcurve. Most observers will catch emission from the two poles if  $\alpha \geq 30^\circ$  (for  $45^\circ \leq \zeta \leq 125^\circ$  on Figure 2). The dark features show the accumulation of photons because of the trailing side caustics (for instance, the thick black curve at  $\zeta < 130^\circ$  and  $|\Phi| < 50^\circ$  behind pole 1), and because of the overlap between the trailing side of pole 1 and the leading side of pole 2 near the light cylinder (for instance, the thinner branch of the Y feature at  $50^\circ < \zeta < 90^\circ$  and  $50^\circ < \Phi < 110^\circ$ ). The main peaks come from the trailing side of each pole, interpeak emission from the leading sides. The thin arcs of emission emanating from each pole are caused by notches in the polar caps distorted by retardation [8], which produces bunching of field lines. Most of the emission takes place at  $0.1 \leq r/R_{LC} \leq 0.8$ .

Being a subset of the slot gap above the null surface, an observer can see only one pole from the outer gap (see

Figure 3). There is no emission outside the sharp peak edges and over a large fraction of the  $\Phi - \zeta$  space. The gaps are invisible at  $\zeta < 30^\circ$  or  $\zeta > 150^\circ$  for any obliquity and they shine only near the equator for small  $\alpha$  inclinations. The dome-like structure in each half of the phase plot is due to the shell-like shape of the trailing field lines. The leading side emission shows up as a smaller dome protruding at lower phase and partially overlapping with the trailing side. Photons emitted on trailing field lines bunch up to form the second peak caustic (similar to the slot gap peaks) while the first peak originates near  $0.9R_{LC}$ . The latter is very sensitive to the assumed gap geometry (length along the lines, thickness across the lines, and height above the last closed lines). It would also disappear for emission very near the edge of the open volume ( $\theta = 0.9\theta_{PC}$ ). It is also very sensitive to the current feedback on the true field configuration. Recent calculations [40] show that the outer gap can extend below the null surface, so wider beams and 2-pole emission are possible as for the slot gap, but the electrodynamics in the slot and outer gap models are quite different.

The phase plots outline the different beaming fractions of the three emission models and the increasing probability of observing radio-quiet objects from the polar cap to the outer gap model because of the small aperture of the radio conal beam near the poles. In the slot and outer gaps, peaks result from the trailing caustic, so one expects well synchronized peaks across the entire spectrum. Phase shifts between the radio core component and the centroid of the conal peaks, as well as polarization patterns, have been used to estimate the altitude of the radio emission: the faster the pulsar, the closer the radiation is to the light cylinder [27]. So, radio waves born on the trailing side high enough to be in the caustic zone would appear in phase with the high-energy photons [22]. Hard X-ray polarization will be a crucial tool to test the caustic role as it implies a drop of the degree of polarization and a double swing by  $180^\circ$  of the position angle within the peak [11].

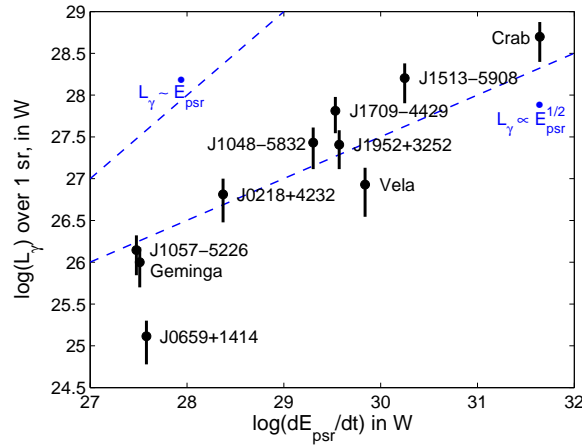


**FIGURE 4.** High-energy luminosity (as measured over 1 sr above 1 keV) vs. spindown power as in [41].

## CLUES FROM OBSERVATIONS

Comparing the lightcurves at different wavelengths for a single object potentially provides a wealth of information on the gap location and on the cascade development and its radiation processes. Spectral cut-offs in  $\gamma$  rays also bear signatures of the pair production mechanism. Compton up-scattered radiation at TeV energies can constrain the number of secondary pairs and their location. The overall luminosity is linked to the rotation power and the maximum  $E_{\parallel}$  field that is not screened along B. Unfortunately, only 9 pulsars (including 1 ms pulsar) are known in  $\gamma$  rays, 10 in the optical and 30 in X rays, and they present an outstanding variety of lightcurve configurations and spectral shapes (see Figure 5). Crab-like objects and several ms pulsars exhibit well synchronized pulses over many decades in energy that suggest very short cascades (within hundreds of meters) or an origin in the caustic zone, whereas the complex and out-of-phase peaks and bumps of Vela-like or PSR B1055-52-like objects suggest the presence of several beams or of a heterogeneous beam with strongly varying spectra. The detection in  $\gamma$  rays of 6 of the 9 radio pulsars with highest  $\dot{E}_{psr}$ -over-square-distance rank indicates a close relationship between the onset of high-energy showers and coherent radio emission, but the existence of Geminga, the only radio-quiet pulsar known so far, proves that the radio and high-energy beams have different apertures or directions. Only the younger ( $< 0.4$  Myr), brighter pulsars have been detected at high energy so far, yet they illustrate how important it is to understand the acceleration and cascading

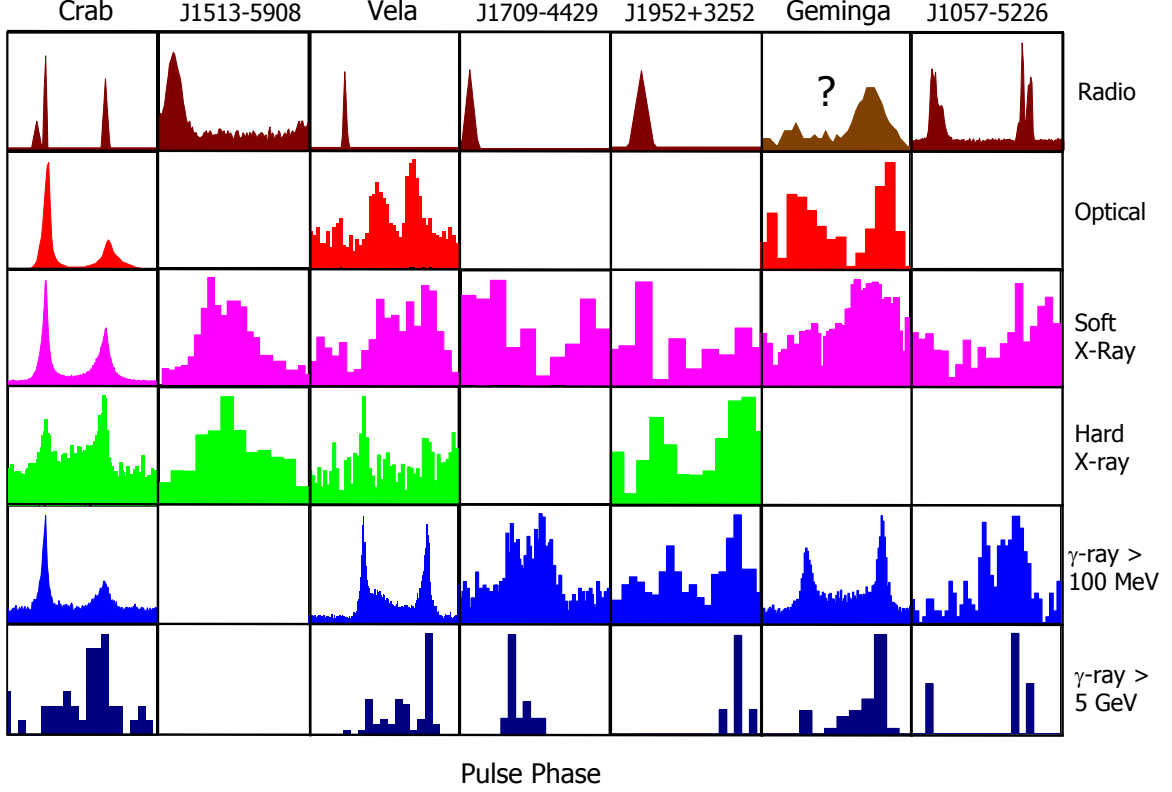


**FIGURE 5.** Light curves of seven  $\gamma$ -ray pulsars in six energy bands, as in Thompson [41].

processes since the  $\gamma$ -ray luminosity clearly dominates the radiation budget. It exceeds the radio luminosity by 6 or 7 orders of magnitude.

$\gamma$ -ray pulsars behave somewhat counter-intuitively: the older pulsars have harder spectra and are more efficient in  $\gamma$  rays. Figure 4 shows that the  $\gamma$ -ray luminosity over 1 sr scales as  $L_{\gamma 1sr} \propto \dot{E}_{\text{psr}}^{1/2}$  over 4 decades in  $\dot{E}_{\text{psr}}$  ([41]), despite the likely dispersion in the true beam apertures. This trend suggests that the cascade current is a constant fraction of the maximum GJ current across the polar caps ( $N_{GJ} = \rho_{GJ} \pi R^2 \theta_{PC}^2 / e \simeq 1.4 \times 10^{32} e^{\pm} s^{-1} (P/0.1s)^{-2} (B_p/10^8 T)$ ) and that the maximum energy  $E_{\text{max}}$  gained in the gap is rather constant and radiated away by the cascade. As discussed above, the feedback between particle acceleration and electrical screening by the cascading yields rather stable  $E_{\text{max}}$  around 10 TeV in both the polar cap [16] and outer gap [25] models. The relation should break for  $\dot{E}_{\text{psr}} < 10^{26}$  W for the  $L_{\gamma}/\dot{E}_{\text{psr}}$  efficiency not to exceed 100%. For older pulsars, the relation should turn to  $L_{\gamma 1sr} \propto \dot{E}_{\text{psr}}$  for both polar cap and outer gap accelerators because of the inefficient electrical screening and of the gap filling a large fraction of the open magnetosphere. Cascading being less efficient, one expects emission from older pulsars to be dominated by hard curvature radiation. This is the case for instance in ms pulsars where, because of the low magnetic field, the unscreened  $E_{\parallel}$  keeps accelerating particles to high altitudes and the resulting curvature radiation, radiation-reaction limited to several tens of GeV, could provide a measure of  $E_{\parallel}$ .

Spectral signatures at very high energies will help distinguishing between models. The overall cascade spectrum and potential asymmetries in the cut-off energy between the leading and trailing side are not discriminant, but the sharpness of the cut-off and its dependence on the magnetic field can be. Emission from the polar cap should abruptly break at energies  $E_{\text{cut}} \propto P^{1/2} B_p^{-1/2} (r/R)^{7/2}$  [21]. The observed dependence between  $E_{\text{cut}}$ , from 20 MeV for PSR B1509-58 to more than 10 GeV for PSR J1951+32, and the surface magnetic field  $B_p$  [41] is compatible with a magnetic origin of the cascade, but the dispersion is large and any conclusion requires more data. Observations above 100 GeV with the HESS telescope cannot distinguish between an exponential and a super-exponential break, yet they start to constrain the amount of inverse Compton radiation produced in the thick outer gap, for instance in Vela [39].

Population studies offer a statistical means to test the radio and  $\gamma$ -ray luminosity dependence on pulsar age and

power, and of the aperture and sweeping properties of the beams. It is evident that a pencil beam from the polar cap, a funnel beam from the slot gap, and a fan beam from the outer gap will sweep differently across the sky and yield different numbers of radio-quiet and radio-loud objects if the radio beam significantly differs from the  $\gamma$ -ray one. This test, however, may turn out to be less conclusive for young pulsars which have high-altitude radio conal beams closer to the high-energy beams [29, 26]. The current studies of radio-quiet and radio-loud statistics using the polar cap and the slot gap models are compatible with the detection by EGRET of 8 radio pulsars, the existence of Geminga, the presence of a score of unidentified EGRET sources along the Galactic plane and of a handful of sources in the Gould Belt [14, 15]. The outer gap can also contribute a large fraction of the unidentified sources at low latitudes [44]. For all models, only the younger (brighter)  $\gamma$ -ray pulsars can be detected above the intense emission from the Milky Way.

In conclusion, many fundamental questions remain open in pulsar twinkling. Observing and modelling a large sample of them at  $\gamma$ -ray and hard X-ray energies with the forthcoming telescopes (AGILE, GLAST, SIMBOL-X) and trying to get polarization data at high energy (PoGO) will bring critical clues and will nicely complement the studies of binary pulsars to understand the electrodynamics of large magnetic fields in strong gravity fields.

## ACKNOWLEDGMENTS

We warmly thank Dave Thompson and Jarek Dyks for their help and time.

## REFERENCES

1. Arons, J. 1983, *ApJ*, 266, 215.
2. Arons, J. & Scharlemann, E. T. 1979, *ApJ*, 231, 854.
3. Cheng, K. S. & Ding, W. K. Y. 1994, *ApJ*, 431, 724.
4. Cheng, K. S., Ho, C., & Ruderman, M. A. 1986, *ApJ*, 300, 500.
5. Cheng, K. S., Ruderman, M. A. & Zhang, L. 2000, *ApJ*, 537, 964.
6. Deutsch, A. J. 1955, *Ann. d'Astrophys.*, 18, 1.
7. Daugherty, J. K. & Harding, A. K., 1996, *ApJ*, 458, 278.
8. Dyks, J. & Harding, A. K. 2004, *ApJ*, 614, 869.
9. Dyks, J. & Rudak, B. 2002, *A & A*, 393, 511.
10. Dyks, J. & Rudak, B. 2003, *ApJ*, 598, 1201.
11. Dyks, J., Harding, A. K. & Rudak, B. 2004, *ApJ*, 606, 1125.
12. Goldreich, P. & Julian, W. H. 1969, *ApJ*, 157, 869.
13. Gonthier, P. G. & Harding A. K. 1994, *ApJ*, 425, 747.
14. Gonthier, P. L., Van Guilder, R., & Harding, A. K. 2004, *ApJ*, 604, 775
15. Gonthier, P. L., Van Guilder, R., Harding, A. K., Grenier, I. A., & Perrot, C. A. 2005, *ApSS*, 297, 71
16. Harding, A. K. & Muslimov, A. G. 1998, *ApJ*, 556, 987.
17. Harding, A. K. & Muslimov, A. G. 2002, *ApJ*, 568, 862.
18. Harding, A. K., Muslimov, A. G. & Zhang, B. 2002, *ApJ*, 576, 366.
19. Harding, A. K. & Zhang, B. 2001, *ApJ*, 548, L37.
20. Harding, A. K., Usov, V.V. & Muslimov, A. G. 2005, *ApJ*, 622, 531.
21. Harding, A. K. 2005, in *High Energy Gamma-Ray Astronomy*, ed. F. A. Aharonian, H. Volk & D. Horns, AIP 745, 105.
22. Harding, A. K. 2005, in *Proc. of 22nd Texas Symp. on Rel. Astrophys.*, ed. P.Chen et al., econf C041213 (astro-ph/0503300).
23. Hibschan, J. A. & Arons, J. 2001, *ApJ*, 554, 624.
24. Hirotani, K. & Shibata, S. 2001, *MNRAS*, 325, 1228.
25. Hirotani, K., Harding A. K. & Shibata, S. 2003, *ApJ*, 591, 334.
26. Johnston, S. & Weisberg, J. M. 2006, *MNRAS*, submitted (astro-ph/0603037).
27. Kijak, J. & Gil, J. 2003, *A&A*, 397, 969.
28. Lyutikov, M. 2005, *MNRAS*, 362, 1078.
29. Manchester, R. N. 1996, in *Pulsar, Problems and Progress*, ed. M.A. Walker & M. Bailes, IAU Coll. 160, ASP, 193.
30. Muslimov, A. G. & Harding, A. K. 2003, *ApJ*, 588, 430.
31. Muslimov, A. G. & Harding, A. K. 2004, *ApJ*, 606, 1143.
32. Muslimov, A. G. & Harding, A. K. 2005, *ApJ*, 630, 454.
33. Muslimov, A. G. & Tsygan, A. I. 1992, *MNRAS*, 255, 61.
34. Petri, J., Heyvaerts, J. & Bonazzola, S. 2002, *A & A*, 384, 414.
35. Romani, R. W. 1996, *ApJ*, 470, 469.
36. Ruderman, M.A. & Sutherland, P. G. 1975, *ApJ*, 196, 51.
37. Spitkovsky, A. 2006, *ApJ*, submitted (astro-ph/0603147).
38. Sturmer, S. D., Dermer, C. D. & Michel, C. F. 1995, *ApJ*, 445, 736.



39. Schmidt, F., et al., Proc. 2nd Int. Symp. on High Energy Gamma-Ray Astronomy, Heidelberg, 2004, APS 745, p. 377
40. Takata, J., Shibata, S., Hirotani, K. & Chang, H.-K. 2006, ApJ, in press.
41. Thompson D. J. 2004, Cosmic Gamma-Ray Sources, ed. K. S. Cheng & G. E. Romero (Kluwer), ApSS, 304 , 149.
42. Zhang, L. & Cheng, K. S. 1997, ApJ, 487, 370.
43. Zhang, L., Cheng, K. S.; Jiang, Z. J.; Leung, P. 2004, ApJ, 604, 317.
44. Zhang, L., Han, Z. X., & Jiang, Z. J. 2005, A&A, 429, 489